IEEE Access
Multidisciplinary | Rapid Review | Open Access Journal

Received May 26, 2020, accepted June 2, 2020, date of publication June 18, 2020, date of current version June 29, 2020.

Digital Object Identifier 10.1109/ACCESS.2020.3003308

A Novel Stationary CT Scheme Based on High-Density X-Ray Sources Device

YITING DUAN, HAITAO CHENG, KAI WANG, AND XUANQIN MOU, (Senior Member, IEEE)
School of Electronic and Information Engineering, Xi'an Jiaotong University, Xi'an 710049, China

Corresponding author: Xuanqin Mou (xqmou@mail.xjtu.edu.cn)

This work was supported by the National Key Research and Development Program of China under Grant 2016YFA0202003.

ABSTRACT With the introduction of cold electron sources such as nanotubes, X-ray sources became small in size so that many sources are installed in array to form stationary CT, which brings benefits of simplicity in mechanism and fast response. However, the nanotube-based X-ray source is still singly packaged and hence density of X-ray sources is limited, which introduces severe sparse-view artifacts and could not be used in practice. With the invention of X-ray sources device based on ZnO nanowires as cold electron emitters, a large amount of X-ray sources is first integrated in a flat panel device. In this study, we design a stationary CT architecture using high-density sources devices, called HD-SCT, and develop corresponding reconstruction algorithm. Specifically, several flat panel detectors and X-ray sources devices are spliced together to form a source-detector plate. Multiple source-detector plates are organized as a polygon that encloses object to complete CT scanning. In HD-SCT, X-ray sources are close to object which can significantly decrease CT device volume. The X-ray beam emitted by each source just cover part of object and the spot sources alternately light to completely scan object. Simultaneously, we propose a reconstruction method for the specific configuration which adopts an iterative algorithm to resolve the reconstruction based on alterative part projections, as well as a novel correction process of projection completion for the shadowed area of placing X-ray source devices. To validate the design of the proposed HD-SCT, we execute a series of simulation experiments, which show that the proposed HD-SCT and corresponding reconstruction method effectively remove the artifacts caused by the embed X-ray source device. The results also disclose that with the increase of density of X-ray sources, the resolution of reconstruction has been dramatically improved, which demonstrates the practical value of introducing high-density X-ray sources device into stationary CT design.

INDEX TERMS Stationary CT scheme, high-density X-ray sources devices, source-detector plate, iterative reconstruction.

I. INTRODUCTION

Cone beam computed tomography (CBCT), including a single cone-beam X-ray source and flat detectors, scans the object by rotating 360° to obtain projection data, and hence reconstruct the inner structures of the object based on the projection. It has been widely used in many applications. However, in conventional CBCT devices, limited with cone angle of thermionic X-ray source, the distance between source and object should be far enough to cover the region of interest (ROI), which results in the large volume of CT device. The imaging system with large volume cannot be tightly coupled with object, which causes dose radiation to non-related areas. Besides, due to the rotation scanning of CBCT, mechanical vibration is inevitable, which will seriously degrade the imaging quality [1], [2].

To overcome the limitation of conventional CBCT devices, in recent years, field emission (FE) X-ray cold electron sources are gradually developed due to their great advantages. By using cold electron cathode tubes, FE sources have faster time response, higher stability, longer lifetime, and lower energy consumption [2]–[6]. For example, cold electron sources based on carbon nanotubes (CNT) have small size, instantaneous response, and can be electronically controlled, make it possible to design linear arrays of X-ray sources, which motivate developing novel CT imaging

The associate editor coordinating the review of this manuscript and approving it for publication was Essam A. Rashed.

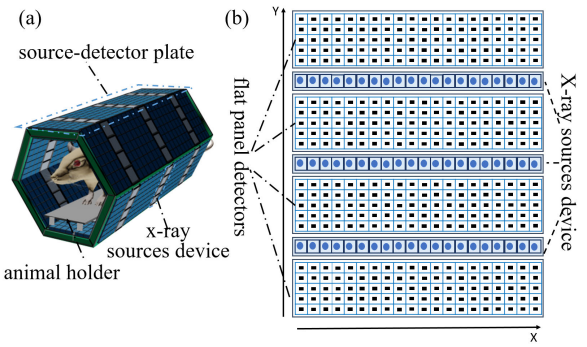

FIGURE 1. System design scheme of stationary CT based on array X-ray sources devices. (a) The whole structure of stationary CT. (b) one source-detector plate.

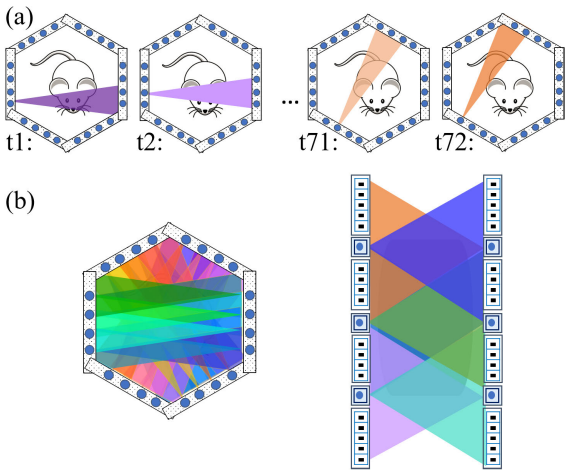

FIGURE 2. (a) An example of scanning process of stationary CT in the central transaxial plane. Assume that each sources device integrates 4 source units, every source-detector plate places 3 X-ray sources devices, which means a total of 72 sources in 6 source-detector plates. Then, from t1 to t72, all X-ray sources emit cone-beam X-ray one after one. (b) The final scanning results of stationary CT in the central transaxial plane and sagittal plane.

schemes [7]–[9]. G. Yang *et al.* developed a stationary digital breast tomosynthesis system with a multi-beam field emission X-ray source array [7]. E. Quan *et al.* designed rotation-free square and hexagonal micro-CT configurations, and proposed a reconstruction method for the designed configuration [8]. B. Gonzales presented a rectangular fixed-gantry CT for airport security inspection system, and developed a compression-based iterative reconstruction method [9].

The above stationary CT imaging architectures make use of X-ray source array based on cold electron cathodes such as CNT, which bring benefits of simplicity in mechanism and fast time response. However, each X-ray source based on carbon nanotube is still singly packaged and hence the density of X-ray sources is limited, which introduces severe sparse-view or limited angles artifacts in CT reconstruction. With severe sparse-view artifacts, polygonal stationary CT system could not be used in practice [10].

With the invention of X-ray sources device based on ZnO nanowires as cold electron emitters, a large amount of X-ray sources is first densely integrated into a flat panel device [11]–[13]. X-ray sources device based on ZnO nanowires not only preserves FE superior properties, but also arranges a large amount of X-ray sources densely into a device, which could be used to efficiently solve sparse-view artifacts existing in the above stationary CT system. Hence, in this study we propose a novel stationary CT scheme based on arrangement of high-density X-ray sources devices using ZnO nanowires field emitters, called HD-SCT.

Based on the high-density integrated X-ray source device, the configuration of the proposed HD-SCT, splices array X-ray sources devices and flat detectors together to form a source-detector plate, organizes multiple source-detector plates as a polygonal columnar that encloses the object to complete CT scanning, as shown in Fig. 1. Such closed polygon-shape structure not only reduces architecture volume, but also avoids unnecessary dose radiation to non-related area. In addition, the dense arrangement in an X-ray sources device can reconstruct the object with high spatial resolution. During the scanning, each source emits a small cone-beam X-ray, which only irradiates a certain part region of object. And all of cone-beams emit one after one to ensure an overlapped coverage for the entire object, as shown in Fig. 2.

In the same time, we propose a reconstruction method for the specific configuration which adopts an iterative algorithm to resolve the reconstruction based on the alterative part projections. Besides, there are missing projection data that is at the region of placing X-ray source devices in the source-detector plate, which will result in artifacts in the reconstructed image [14], [15]. Due to the width of the X-ray source device is in millimeter level, which is much higher than the pixel size of the detector, the conventional artifact deduction methods, such as interpolation [16], [17], regularization in iterative reconstruction [18] cannot handle it well. In this regard, we propose a data completion method to compensate the lost projection. Specifically, combined with interpolation reconstruction and direct reconstruction, we put forward a correction method based on a combined prior information to complete missing projection data.

In this study, we initiatively design a novel stationary CT scheme based on recently proposed high-density array X-ray sources configuration using ZnO nanowires as cold electron emitters, called HD-SCT. In the design of HD-SCT, we splice flat panel detectors and array X-ray sources devices together to form a source-detector plate, and then organize multiple source-detector plates as a polygonal columnar to enclose the scanning object. The proposed HD-SCT architecture not only retains the huge advantages of stationary CT, such as fast response, low radiation, stationary scanning, and so on, but also solves the problem of sparse-view artifacts in CT reconstruction. Based on this closed polygonal architecture, we design specific scanning scheme and then develop

corresponding reconstruction algorithm including iterative reconstruction and projection completion method. Finally, we validate the proposed HD-SCT configuration by a series of simulation experiments based on a hexagonal columnar geometry.

II. METHOD

A. SYSTEM DESCRIPTION

The proposed HD-SCT system configuration is composed of six source-detector plates, which enclose the scanned object to form the structure of regular polygonal columnar. The schematic diagram of the system is shown in Fig.1. Each source-detector plate is formed by splicing flat detectors and array X-ray sources devices. Adjacent source-detector plates are connected by a hinge structure that can easily wrap the object. Specifically, a large amount of X-ray sources with high-density arrangement are integrated into a flat panel device, and then X-ray sources devices combine with flat panel detectors to make up source-detector plate. In every source-detector plate, several X-ray sources devices are distributed in an array with the equal space.

Different from conventional CT architecture, which only use a single X-ray source, the proposed HD-SCT architecture use high-density X-ray sources devices, which contain a large amount of X-ray sources. For the specific CT configuration, the scanning scheme is designed as follows. During scanning, every source emits a cone-beam X-ray, which only covers a small certain part region of object, as shown in Fig. 2(a), and all of cone-beams are emitted one after one to have an overlapped coverage for the entire object, as shown in Fig. 2(b). By making use of individual addressable character and ultra-switch time of field emission cathode [12], the spot sources alternately light to completely scan the object. And it is ensured that every flat detector does not receive two or more X-ray sources simultaneously which will result in overlapped scanning area.

Due to the specific CT configuration, the proposed HD-SCT structure exists detection blind zones, which are located at the regions of placing X-ray source devices in the source-detector plate, as shown in Fig.1. Therefore, we need raise up a corresponding correction method to complete the missing projection data. Zhang *et al.* have proposed a metal artifact correction method, which utilizing original reconstruction and corrected reconstruction by linear interpolation to finish image mutual correction [19]. Inspired by this idea, by exploiting the advantages of missing projection and interpolation projection, we can fill up the missing projection data based on combined prior information.

The working procedure of the proposed HD-SCT configuration can be divided into the following steps. First, we place the scanned object in the CT architecture. Second, X-ray sources scan object alternately, and detectors located at the opposite plate receive projection data until all the spot X-ray sources are lighted. Third, we fill up the missing projection data, which is located at the shadowed area of placing X-ray source devices in the source-detector plate. Last, according to the physical model of scanning process, we construct object function and reconstruct image iteratively. Through above steps, we can obtain the volume reconstruction of the scanned object.

The characteristics of HD-SCT mainly contains four parts. (1) The CT system surrounds the object with a polygonal columnar. It doesn't need rotate to finish scanning, which not only reduces the complexity of mechanical design, but also avoids the effects of mechanical vibration during rotation process. (2) By using high-density X-ray sources devices, each source doesn't need completely cover the scanned object. That credibly reduces the distance between X-ray sources and the object. Besides, the size of imaging architecture can be significantly reduced, which shows great potential on applying the system to practical applications. (3) This special structure enables tight coupling of the object with the scanning system. It effectively reduces the dose radiation to non-related areas during the scanning process. (4) More importantly, we make use of the high-density X-ray sources device into HD-SCT design, which can significantly reduce sparse-view artifacts in reconstruction compared to other stationary CT schemes, which will be investigated in this study.

B. RECONSTRUCTION

1) FORWARD AND BACKWARD PROJECTION ALGORITHM

Due to lighting the spot sources alternately, the projection data is considered to be un-mixed. Therefore, we can construct the forward projection model as what conventional CT does. In conventional X-ray radiation, we combine air scanning to obtain actual projection data. In forward projection, we assume that all X-ray sources were monochromatic and detectors were considered ideal. When the q^{th} source lights, the measured photon counts in p^{th} detector unit can be written as:

$$\hat{y}_{pq} = I_{pq} \exp(-a_{pq}x) + n_p. \tag{1}$$

where I_{pq} are the emission counts from $q^{th}(q = 1, \cdots, Q)$ source to opposite $p^{th}(p = 1, \cdots, P)$ detector, P is the number of detector units and Q is the number of sources in one source-detector plate, $\hat{y}_{pq}$ is the expected measurement of response photon number from q^{th} source to opposite p^{th} detector, a_{pq} is the length along the X-ray path, x is the object attenuation coefficient and n_p is the random noise.

In the above projection, due to the detection blind zones of the proposed HD-SCT architecture, the projection data is incomplete and partly missing. The corresponding completion method will be introduced in the next subsection.

To obtain the internal structure for diagnostics or evaluation with the projection data from the geometry, a reconstruction algorithm is proposed. The objective function of the reconstruction is as follows:

$$\min_x \sum_{p=1}^{mP} \sum_{q=1}^{Q} \|a_{pq}x - \hat{b}_{pq}\|_2 + \lambda R(x). \tag{2}$$

where m is the number of source-detector plates, $\hat{b}_{pq} = \log \frac{I_{pq}}{\hat{y}_{pq}}$ represents the linear integral value along the X-ray path from q^{th} source to opposite p^{th} detector. The first term indicates the data fidelity in the $l2$-norm. The second term consists of $R(x)$ as a regularization function. The parameter λ controls the balance between the fidelity and the regularization [20], which is selected empirically.

For the optimization of objective function, we solve it by an iterative reconstruction method. Each iteration includes two phases to solve data fidelity and regularization term separately. Assuming the data fidelity is $f(x)$, then we update reconstruction image iteratively by gradient descent method as follows [21]:

$$x^{k+1} = x^k + \alpha \frac{f'(x^k)}{f''(x^k)}. \tag{3}$$

where x^{k+1} and x^k are the iterative results, $f'(x^k), f''(x^k)$ are the first derivative and second-order derivative, respectively, and α is relaxation factor.

For the regularization term, we employ TV algorithm [18] as $l1$-norm constraint to reduce total variation of the image estimate. Meantime, to improve the speed of iterative convergence, we adopt Nesterov's momentum acceleration strategy to speed up the convergence [22].

2) PROJECTION COMPLETION ALGORITHM

We adopt a correction method based on combined prior information to complete missing projection data. The main procedure of correction is shown in Fig. 3, which can be described in details as follows:

(1) Linear Interpolation. Interpolate the projection data in the missing region of the original projection P0 to obtain interpolation projection P1.

(2) Pre-reconstruction. Iteratively reconstruct the original projection P0 and interpolation projection P1 to obtain an uncorrected reconstructed image F0 and an interpolated corrected reconstructed image F1.

(3) Artifacts splitting. The original image F0 can be regarded as the ground truth image plus an artifacts image caused by missing data, and the interpolated corrected image F1 can be treated as the ground truth image plus an artifacts image caused by interpolation data. Therefore, the difference of these two reconstructed images, F0-F1, represents the superposition of artifacts with missing data and the interpolation data.

(4) Threshold segmentation. Selecte a suitable threshold to divide the artifacts superposition image so as to obtain a strong artifacts map.

(5) Correlation map. Image mutual correlation can be used to evaluate the degree of similarity of two images [23]. The mutual correlation of two vectors x and y can be calculated as follows:

$$C(x, y) = \frac{2\langle x, y\rangle + \epsilon}{\|x\|^2 + \|y\|^2 + \epsilon}. \tag{4}$$

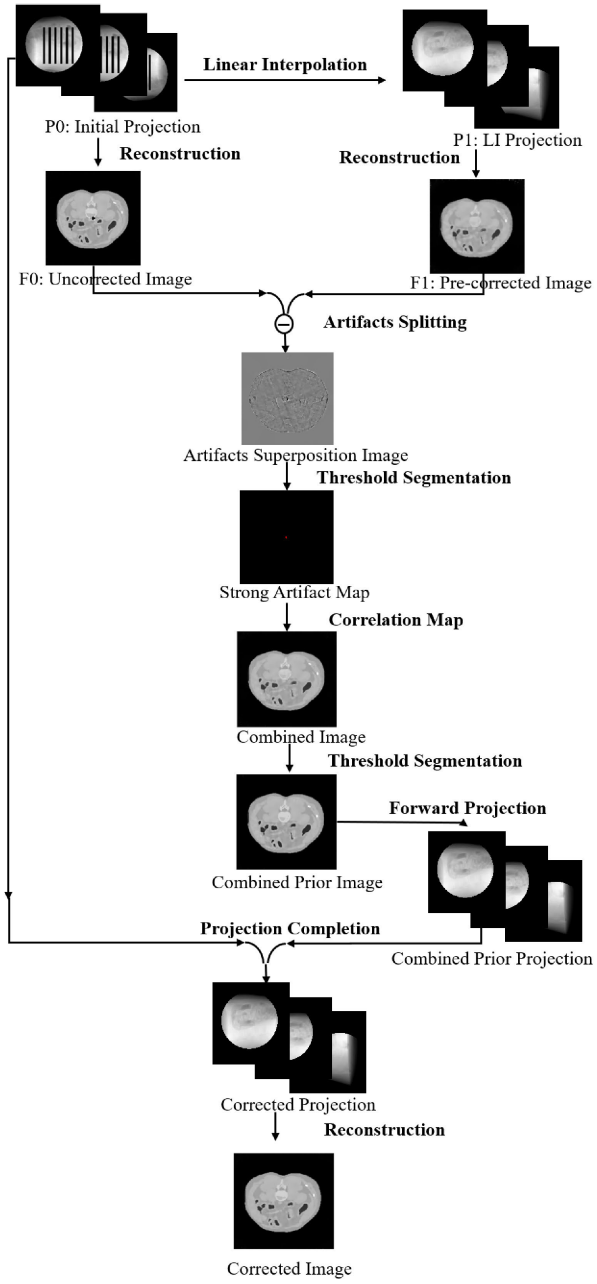

FIGURE 3. The correction procedure of HD-SCT based on combined prior information.

where symbol $\langle \cdot, \cdot \rangle$ represents the inner product, and ϵ is a small positive constant to make sure that the denominator is not zero.

We calculate the mutual correlation of the artifacts image blocks and F0, F1 respectively. The larger the correlation coefficient is, the more similar we consider their structure to be, which indicates the artifacts blocks are mainly from the more similar blocks of image. For example, if the correlation coefficient of a certain artifact block and F1 is higher, the artifact is more likely to be caused by interpolation data. In this case, F0 is likely to contain fewer artifacts and is selected

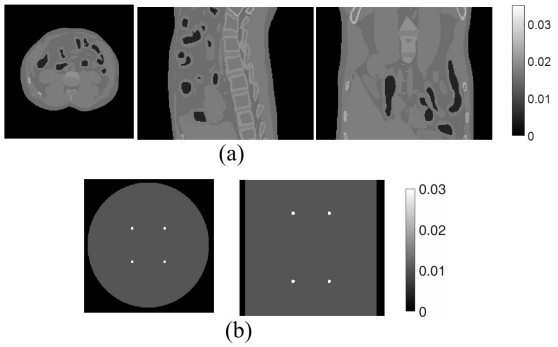

FIGURE 4. Two phantoms used in the simulations. (a) The chosen transverse (left), sagittal (middle) and coronal (right) planes of the XCAT phantom. (b) The transverse (left), sagittal (right) planes of the designed phantom.

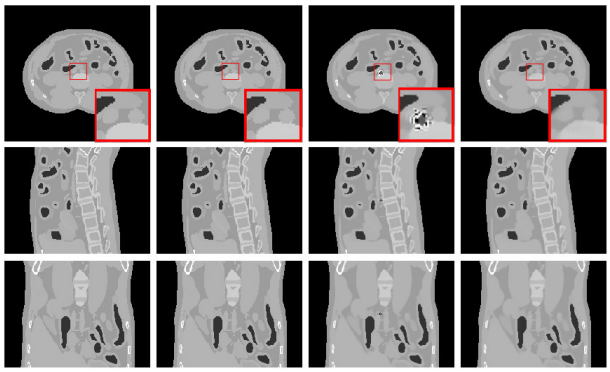

FIGURE 5. Reconstruction of HD-SCT based on combined prior information. The first column is the ground truth, the second column is the ideal reconstruction without missing projection, the third column is the direct reconstruction with missing projection, and the last column is the reconstruction based on combined prior information. Display window is [0, 0.035].

to build the combined image; otherwise, F1 is chosen. If an artifact image block with both low correlations to F0 and F1, F1 will be selected by default. After that, a smooth transition in the combined image is needed.

(6) Generation of combined prior image. Segment the combined image into different material tissues, each of which is assigned a uniform value. Therefore, we can obtain the combined prior image.

(7) Projection completion and image reconstruction. Complete the missing data of the original projection and make a smooth transition, and then we can get the final corrected projection.

After obtaining the final corrected projection, we can reconstruct the image based on the iterative algorithm.

III. EXPERIMENT

A. EXPERIMENTAL MATERIALS

In this study, we adopt simulation experiments to quantitatively analyze the performance of the proposed CT configuration and corresponding reconstruction algorithm. Specifically, we investigate the effect of the density of X-ray sources on the reconstruction quality. We use two phantoms for evaluation. The first phantom is XCAT phantom [24], as shown in Fig. 4(a). The structure of XCAT has enough structural features to fully evaluating the reconstruction performance of the proposed CT configuration. The second phantom is our designed uniform cylinder, in which eight spheres of 1mm are inserted symmetrically, as shown in Fig.4(b). Such a simple multi-sphere phantom is used to analyze spatial resolution in HD-SCT reconstruction.

The purpose of this study is to validate the feasibility of the proposed CT configuration and explore the reconstruction performance. Hence in the simulation experiments, we assume that all X-ray sources were monochromatic and detectors were considered ideal. The size of the phantom is $256 \times 256 \times 200$ with a voxel size of 0.25 mm $\times$ 0.25 mm $\times$ 0.25 mm. The distance between two opposite source-detector plates is 100 mm. Without considering the detection blind zones in the source-detector plate, the flat detectors have a dimension of 900×800 with a resolution of 0.2 mm $\times$ 0.2 mm. There are four X-ray sources devices with adjacent distance 12 mm in every source-detector plate, and each sources device integrates 64 X-ray sources with 0.8 mm adjacent space. The width of missing projection is set 2mm, which is suitable for the currently developed device. During scanning, each source irradiates a narrow cone beam X-ray with same cone angle of 45°, which is easily implemented in the currently developed X-ray sources device.

B. RECONSTRUCTION RESULTS

1) ITERATIVE RECONSTRUCTION WITH PROJECTION COMPLETION

Based on the proposed HD-SCT scheme, we use the XCAT phantom to perform forward projection based on formula (1), and then complete iterative reconstruction based on formulas (2) and (3). The results of reconstruction are shown in Fig.5. Among them, the first column shows the reference image, the second column shows the ideal reconstruction when the projection data is assumed to be complete and un-missing, the third column shows the direct reconstruction when the projection data is partly missing, and the last column shows the final reconstruction when the projection data is corrected based on projection completion algorithm. We can easily find that the ideal reconstruction without missing projection is of highly quality, which shows the reliability of the HD-SCT scheme. Considering the missing projection located at the occlusion area of placing X-ray source devices in the source-detector plate, the reconstruction exists evident artifacts in the center part, such as structure missing and blurring, as shown in the third column. After the correction based on combined prior information, these artifacts reduce considerably, which indicates that the proposed correction method is effective to solve artifacts caused by missing projection, as shown in the last column.

To quantify the reconstruction image quality before and after projection completion, we evaluate the reconstructed

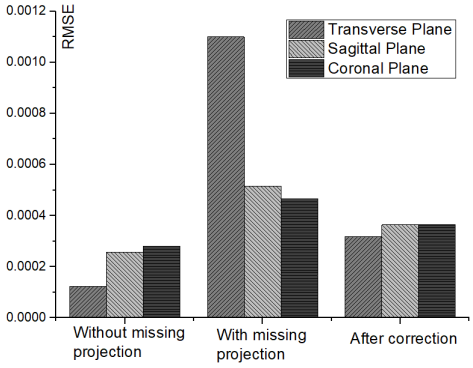

FIGURE 6. RMSE of different reconstruction results.

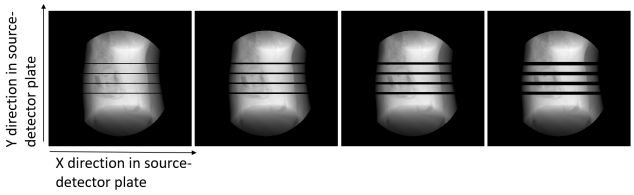

FIGURE 7. A group examples of projection for different missing projection widths. From left to right, the missing widths are 1mm, 2mm, 3mm, and 4mm.

phantom by the root mean square errors (RMSE). The results are shown in Fig.6. It confirms that the correction based on the combined prior information really reduces artifacts caused by the missing projection and improves the image quality. Therefore, applying the proposed CT system to practice is feasible.

2) INFLUENCE OF PROJECTION MISSING WIDTH

During forward projection, the width of missing projection caused by placing X-ray source devices decides the loss rate of the valid information. We define loss rate as the ratio of number of missing projection pixels to number of ideal projection pixels. Keeping other system parameters as the same, under the normal dose scanning, we set projection missing width to be 1mm, 2mm, 3mm and 4mm respectively. Then, the corresponding loss rate is 3.5%, 7.0%, 10.5% and 14%, respectively. The sample is shown in Fig.7.

Fig.8 shows iterative reconstruction results about XCAT phantom using corrected completion projection under different projection missing widths, which illustrates the proposed projection completion algorithm can basically recover the information of missing projection. As the width of the missing projection increases, the quality of reconstruction gradually decreases, which is reflected in the blurring effect of the image edge and disappearance of small tissue structures. When projection missing width is more than 2mm, severe trailing artifacts appear in the center of the reconstruction, as indicated by the red boxes.

Table 1 shows the RMSE and contrast to noise ratio (CNR) values of reconstruction with different projection missing widths about XCAT phantom. We calculate CNR in two regions, which are marked by yellow boxes in Fig.8. It can be

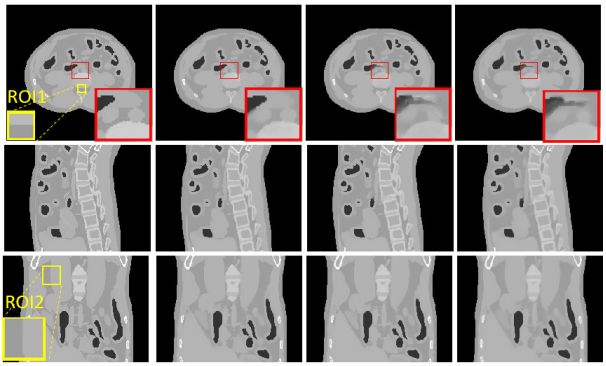

FIGURE 8. Reconstruction results using corrected completion projection under different projection missing widths. Projection missing width from left to right is 1mm, 2mm, 3mm and 4mm respectively. Display window is [0, 0.035].

TABLE 1. RMSE and CNR of reconstruction with different projection missing widths.

Missing Width		0mm	1mm	2mm	3mm	4mm
RMSE (× 1e-4)	Transverse	1.24	1.30	3.18	5.55	6.17
	Sagittal	2.57	2.78	3.38	3.92	6.53
	Coronal	2.80	2.86	3.23	3.69	6.30
CNR	ROI1	31.57	28.01	22.00	7.23	3.67
	ROI2	49.89	46.73	40.08	24.29	14.74

seen that as the projection missing width increases, the RMSE value gradually increases and the CNR value decreases, which indicates that the reconstruction quality gradually is gradually getting worse. When the projection missing width is less than 2mm, the reconstruction quality is close to the ideal reconstruction; and after larger projection missing width, the reconstruction quality is significantly reduced. Therefore, the proposed projection completion algorithm is more suitable for iterative reconstruction with projection missing width less than 2mm.

3) NOISE PERFORMANCE

In real X-ray scanning, due to the interaction of X-ray with phantom, the photon intensity received by the detector is a random value, in statistics which is called "Poisson noise". Assuming all X-ray sources are monochromatic, the level of Poisson noise will increase as the number of photons decreases. Keeping other system parameters as before, we set different noise levels to analyze the effect of noise on reconstruction quality about XCAT phantom.

Fig.9 shows the iterative reconstruction results using unmissing projection and corrected completion projection with two noise levels of 50k and 10k, respectively. These two noise levels represent high-dose and low-dose scanning situations, respectively, from which we can observe the robustness of the proposed projection completion algorithm to noise. It can be seen from Fig.9 that there are no obvious artifacts in the reconstruction results. However, observing the details of the image label by red boxes, as the noise level increases, the reconstruction appears slightly blurring effect and reduced resolution.

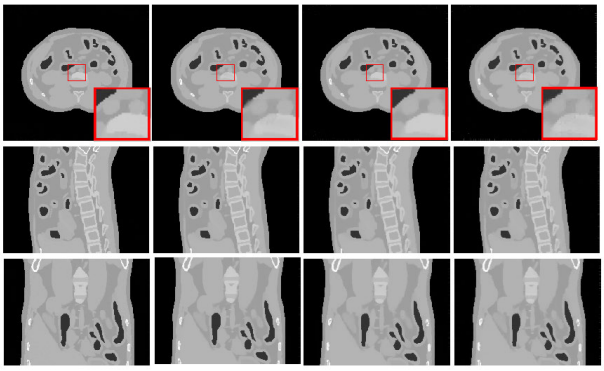

FIGURE 9. Reconstruction results using un-missing projection and corrected completion projection with different noise levels. The first column is ideal reconstruction without missing projection (50K photons), the second column is the reconstruction based on combined prior information (50K photons), the third column is ideal reconstruction without missing projection (10K photons), the last column is the reconstruction based on combined prior information (10K photons). Display window is [0, 0.035].

TABLE 2. RMSE and CNR of reconstruction with different noise levels.

Reconstruction quality		50k photons		10k photons	
		Ideal Recon	Combined Recon	Ideal Recon	Combined Recon
RMSE		2.72e-4	3.52e-4	4.51e-4	6.12e-4
CNR	ROI1	21.41	18.94	11.51	8.90
	ROI2	39.27	32.86	15.78	13.90

Then, we calculate RMSE and CNR values of reconstruction with different noise levels, as shown in Table 2. With the increase of noise levels, the RMSE increases, and the CNR decreases, which indicates that the reconstruction quality of XCAT phantom get worse under the effect of noise. Besides, it can be found that the RMSE and CNR values of reconstruction using un-missing projection and corrected completion projection are almost close under the same noise level. Therefore, we can conclude that the projection completion algorithm based on combined prior information is robust for different noise levels.

4) SPATIAL RESOLUTION

For the proposed HD-SCT, we analyze the spatial resolution of reconstruction based on the designed multi-sphere phantom. The multi-sphere phantom consists of eight spheres of 1mm diameter, which can be considered as points to measure full-width at half-maximum (FWHM) of point spread functions (PSF) and modulation transfer function (MTF) by taking the Fourier transform of the PSF. The FWHM is measured at 50% whereas the MTF is measured at 10%. Therefore, the loss of resolution can be measured by the average FWHM and MTF of eight points. Besides, RMSE is used to measure the overall reconstruction of the multi-sphere phantom. Keeping other system parameters as before, we reconstruct the designed phantom under different noise levels, which are noiseless, 50k photons, and 10k photons, respectively.

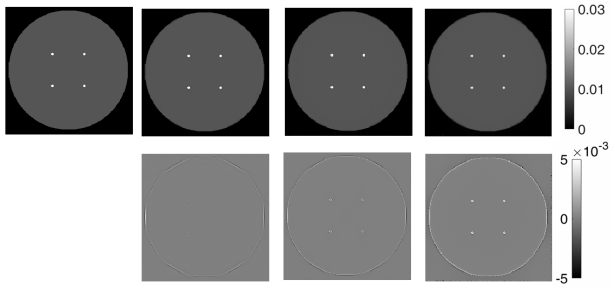

FIGURE 10. Reconstructions and residual maps in the transverse plane of the multi-sphere phantom. The first column is the reference, the second column is the reconstruction without noise, the third column is the reconstruction with 50k photons, and the last column is the reconstruction with 10k photons.

TABLE 3. Image quality metrics about reconstruction of multi-sphere phantom.

Metrics	RMSE	FWHM(mm)	MTF(mm^{-1})
no-noise	2.05e-4	1.12	3.16
50k photons	3.07e-4	1.14	3.15
10k photons	4.40e-4	1.21	2.98

Fig. 10 shows reconstruction slices and the corresponding residual maps under different noise levels. According to Fig. 10, it can be found that under these three kinds of noise levels, the sphere points can be reconstructed well. However, by observing the residual maps, the reconstructed errors increases as the noise level increases, which are mainly reflected in the edge of the cylinder and the spheres.

Then, we calculate the average FWHM, MTF and RMSE of these reconstruction about the designed phantom. The results are shown in Table 3. As the noise increases, the overall reconstruction quality of the designed phantom decreases. According to the average FWHM and MTF values of the eight sphere points, it can be concluded that when the noise level increases, the spatial resolution of the reconstructed sphere points just decrease a little, which indicates that the reconstruction algorithm only sacrifices the spatial resolution to a small extent while suppressing noise to make a balance between resolution and noise.

C. PARAMETERS COMPARISON

In order to better design the HD-SCT scheme, we conduct comparative experiments on different system parameters, including the arrangement density inside each X-ray sources device, the number of X-ray sources devices in a source-detector plate, and the distance between X-ray sources devices.

1) THE DENSITY OF EACH X-RAY SOURCES DEVICE

We consider different densities inside each sources device to study what they impact on reconstruction. Assuming the length of X-ray sources device is fixed, we set the source units inside each X-ray sources device as 8, 16, 32, 64, 128, 256, 512, where the distance between adjacent units are 6.4mm, 3.2mm, 1.6mm, 0.8mm, 0.4mm, 0.2mm, 0.1mm, respectively. The number of X-ray sources devices

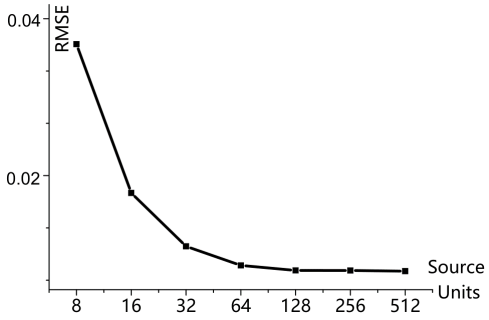

FIGURE 11. RMSE curve of reconstruction and reference under different densities inside each X-ray sources device.

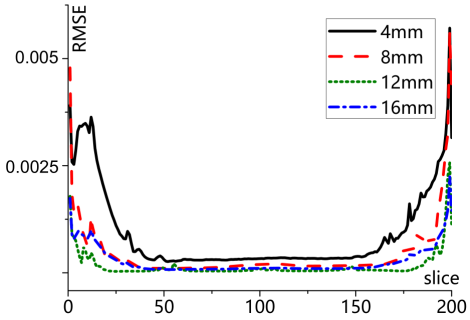

FIGURE 12. RMSE curve of reconstructed slices and reference slices under different distances between X-ray sources devices.

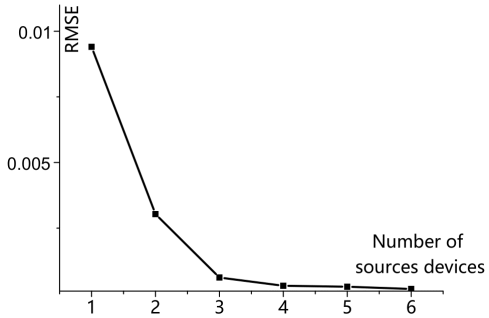

FIGURE 13. RMSE curve of reconstruction and reference under different numbers of sources devices in a source-detector plate.

in a source-detector plate is set as 1. Then, keeping other system parameters same as initial settings, we reconstruct XCAT object by the above parameters.

Fig. 11 shows how RMSE value between the reconstruction results and the reference changes under different parameter settings. From it, we can find that with the source units inside each X-ray sources device increases, the RMSE value gradually decreases, indicating that the reconstruction quality is getting better and better. The source units set as 64 is the turning point of the overall curve. At this point, the reconstruction algorithm has the greatest benefit, that is, both high reconstruction quality and low computational complexity. Therefore, we select the source units inside each X-ray sources device as 64, where the distance between adjacent units are 0.8mm.

2) THE DISTANCE BETWEEN X-RAY SOURCES DEVICES

In order to study the influence of the distance between sources devices on reconstruction, we experiment on the proposed HD-SCT structure. Keeping other system parameters as before, we set the number of sources devices set as 4, and adjust the distances between sources devices as 4mm, 8mm, 12mm, and 16mm. In each X-ray sources device, 64 source units with the distance 0.8mm between adjacent units is used.

We calculate RMSE between reconstructed slices and reference slices, as shown in Fig.12. Therefore, we find that the distance between sources devices does not obviously affect the reconstructed quality. However, as the distance increases, the sources device is more evenly distributed in the source-detector plate, which can consider the whole reconstruction more equally so that the RMSE values in marginal slices are smaller. Therefore, we think the distance between sources devices should depend on the number of sources devices.

3) THE NUMBER OF X-RAY SOURCES DEVICES

The number of X-ray sources devices in a source-detector plate could also impact reconstruction quality. Keeping other system parameters as the same, we set 64 source units inside each X-ray sources device with the distance 0.8mm between adjacent units, which is easily implemented in the currently developed device. Then, we adjust the number of sources devices to 1, 2, 3, 4, 5, 6 in a source-detector plate to find the most suitable numbers about sources devices. Correspondingly, depending on the number of sources devices, we set the distance between each two adjacent sources devices are 0mm, 24mm, 16mm, 12mm, 10mm, 8mm, respectively to ensure the sources devices distributed more evenly in the source-detector plate. Then we reconstruct XCAT object by the above parameters. The values of RMSE between reconstruction and reference are shown in Fig.13. It can be seen from Fig.13 that when the number of sources devices is changed from 1 to 6, the reconstruction quality has increasingly improved. The number of sources devices in the source-detector plate set as 4 with the interval space 12mm is the turning point of the overall curve. At this point, the reconstruction algorithm has the greatest benefit, that is, both high reconstruction quality and low computational complexity. Therefore, we suggest the number of sources devices in a source-detector plate set as 4 with the interval 12mm for reconstruction in the proposed HD-SCT.

D. STRUCTURE COMPARISON

Conventional cone beam computed tomography (CBCT), including a single thermionic X-ray source and flat detectors, scans the object by rotating 360° to obtain projection data, which has great applications in practice. With the introduction

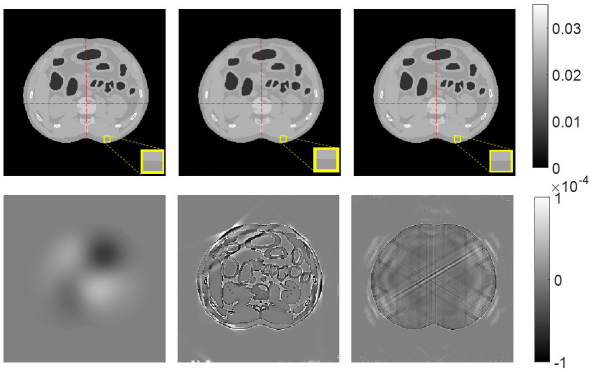

FIGURE 14. Reconstruction slice and the corresponding residual map by these three structures. The system structures from left to right are from CBCT, SCT, and the proposed HD-SCT. Display windows of reconstruction and residual are [0, 0.035] and [-1e-4,1e-4].

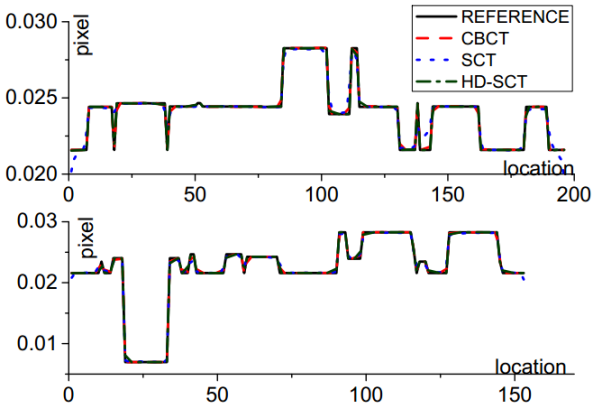

FIGURE 15. Pixel curves, labeled by red dotted lines in Fig. 14. The first group is plotted by row pixels; the second group is plotted by column pixels.

of the structure of the X-ray source array, some researchers have designed a stationary CT structure, called as SCT in this study, which is hexagon-shape consisting of six detecting plates [8]. In the configuration of SCT, three source arrays based on CNT, each consisting of 30 sources, form three contiguous sides of the hexagon and three area detectors form the other three sides. The source units in source arrays are flashed one by one, and the corresponding detectors on the other side receive projection data.

To analyze the differences among these two structures and the proposed HD-SCT, we perform a structural comparison experiment. In the proposed HD-SCT, source units inside each X-ray sources device are set as 64, where the distance between adjacent units are 0.8mm. The number of X-ray sources devices in a source-detector plate is set as 4, where the distance between each two adjacent sources devices are 12mm. In order to compare structure differences among these three structures, we need ensure same projection photons during scanning. Hence, in SCT, it is assumed that 512 source units are distributed in three contiguous sides of the hexagon with the resolution of 0.2 mm (such source density cannot be achieved in the original SCT). In the conventional CBCT, about 400-angles of projection data are evenly obtained to ensure the same number of projection photons during scanning. Besides, due to a single source in CBCT, to completely cover the scanning object, the distance between the single source and flat detectors is set as 150mm, and the distance between center of rotation and flat detectors is set as 50mm. Keeping other system parameters as the same, we reconstruct XCAT phantom by such three structures.

Fig.14 shows one reconstruction slice and the corresponding residual map by these three structures. According to the reconstruction slice, we can find that the scanning object can be reconstructed by these three structures. For the reconstruction of CBCT, SCT, and HD-SCT, we calculate CNR values about a small region marked by yellow boxes in Fig.14. The CNR values of CBCT, SCT, and HD-SCT are 38.52, 30.90 and 35.42, respectively, which indicates the region quality of CBCT is better than the other two, and SCT's region quality is the worst. In addition, we show the corresponding residual map to analyze the various artifacts caused by such three structures. Specifically, the artifacts of CBCT are more evenly distributed and not severe. The blurring artifacts of SCT are the most serious, which are mainly caused by the limited angles scanning. In comparison, the results of the proposed HD-SCT has clearly reconstructed edge structures while exist slight streaking artifacts. In general, the image quality reconstructed by CBCT and the proposed HD-SCT is quite close, and the image reconstructed by SCT exists severe sparse-view artifacts and may not be used in practice.

In order to observe the difference between the reconstruction and the ground truth, we plot pixel curves according to the reconstruction pixels labeled by red dotted lines in Fig.14. The pixel curves are shown in Fig.15. It can be found that such three structures can reconstruct the original values well in the smooth region. However, at the location of edge structure, the pixel reconstructed by CBCT and the proposed HD-SCT is closer to the reference value. The reconstruction by the SCT is slightly worse, implying that it cannot exactly catch fast changes of pixel intensities.

Finally, to more comprehensively compare the differences between SCT, HD-SCT and CBCT, we quantify and analyze the reconstruction quality under different system structural parameter settings, including the system configurations we mentioned above, as well as CBCT having 200,150,100 rotation angles. The RMSE curve at different reconstruction slices is shown in Fig.16. In Fig.16, in addition to reconstructions of three different structures we have mentioned above, we also add reconstructions of CBCT with 200, 150 and 100 rotation angles to compare.

According to the RMSE curve in Fig.16, the image reconstructed by the HD-SCT is of higher quality compared to what reconstructed by SCT. Due to same number of X-ray sources such two structures have, we consider different reconstruction results are caused by the differences between such two structures. Sources are distributed in all sides of the hexagon

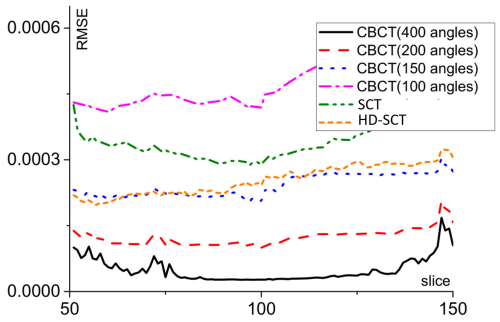

FIGURE 16. RMSE curve of reconstructed slices and reference slices under different system structural parameter settings.

in the proposed HD-SCT while they are only distributed in half sides in the SCT. That means the proposed structure is better to reconstruct images with high quality. Moreover, in the original structure of SCT, X-ray source can hardly be distributed densely, which probably lead to severe sparse-view artifacts in reconstruction.

Comparing conventional CBCT with the proposed structure, the reconstruction by CBCT with 400 rotation angles is better than ours, which means reconstruction by CBCT is better under the same projection photon numbers. The image quality reconstructed by the proposed structure is only equivalent to the reconstruction quality of CBCT with 150 rotation angles. However, in practice, conventional CBCT has problems of mechanical vibration and motion artifacts caused by long-time scanning [25], which will degrade the reconstruction quality. Instead, the HD-SCT configuration with high-density X-ray sources devices doesn't have above problems and still has the potential to achieve better reconstructed image quality.

IV. DISCUSSION

First, we have analyzed the reliability of the proposed HD-SCT scheme. Specifically, we utilized combined prior information to fill up the missing projection and then finished reconstruction. Experimental results show that the reconstruction based on combined prior information is effective and feasible. Besides, the proposed projection completion algorithm based on combined prior information is robust for different noise levels when the projection missing width no more than 2mm.

Second, we have investigated to select the suitable system configuration parameters through multiple comparison experiments, which can provide guidance for building the practical CT system. Experiments show that the reconstruction quality has been greatly improved with the increase of the density of X-ray sources. Considering both computation time and reconstruction quality, we selected the source units inside each X-ray sources device as 64 with the interval distance 0.8mm, and set the number of sources devices in a source-detector plate as 4, where the distance between each two adjacent sources devices are 12mm.

Third, to illustrate the characteristics of the proposed CT structure, we have compared it with two different structures, i.e., conventional CBCT and SCT. By the experimental results, the proposed HD-SCT structure can reconstruct the image with higher quality compared to what reconstructed by SCT. On the other hand, the image quality reconstructed by the proposed HD-SCT is only equivalent to the reconstruction quality of CBCT with 150 rotation angles. However, it is worth noticing that, in practice, the proposed HD-SCT doesn't suffer from mechanical vibration problems and motion artifacts caused by long-term scanning, both of which may occur in CBCT and SCT. Thus, the proposed HD-SCT still has the huge potential to achieve better reconstructed image quality.

The proposed HD-SCT utilizes a large amount of cold sources based on ZnO nanowires to finish stationary scanning. Due to individual addressable character and ultra-switch time of these cold sources, the temporal resolution of HD-SCT may be higher than other rotational CT systems as long as the detector frame-rate can be fast enough. And, in real implementation, it is not limited to the only form of switching on the sources one by one. Another equivalent option is to divide all the sources into several groups as small as possible, and there are no intersected parts in projection data when switching all sources in any groups. In this way, the scanning time of HD-SCT can reduce further.

Further more, in real implementation, the hexagonal HD-SCT structure utilizes X-ray sources device and flat-panel detectors to make a complete device, which can be implemented in currently developed device. And six source-detector devices are organized as a polygon that encloses object to complete stationary CT scanning. The whole scanning process is a stationary imaging, which does not need mechanical rotation or vibration. In this way, HD-SCT system reduces the hardware cost of complicated machinery design, which is inevitably the most difficult part in conventional CT configurations. Besides, the rotational CT configurations usually have a larger imaging volume, which also increase the hardware cost. Hence, the cost of proposed HD-SCT system can be expected to be much lower than the current CT systems. In addition, respiratory motion is a very important issue in CT reconstruction. Although the proposed HD-SCT may have high temporal resolution, which may reduce the artifacts caused by respiratory motion to some extent, the problem of respiratory motion still cannot be ignored. Some researchers have proposed effective algorithms to solve the artifacts caused by respiratory motion in CBCT [25], [26], which will be helpful to settle this concern. In the future work, we will strengthen the research on solving respiratory motion problem in HD-SCT. Furthermore, for the application of real system, low X-ray dosage is very important, and we will study it in depth after the real equipment is finished.

V. CONCLUSION

In summary, we design a stationary CT scheme based on high-density X-ray sources devices using ZnO nanowires as

cold electron emitters. In the proposed HD-SCT configuration, we use multiple source-detector plates to form a polygonal structure so as to avoid mechanical rotation during the scanning. In each plate, high-density X-ray sources devices and flat detectors are spliced together. This specific design significantly solves the problem of sparse-view artifacts in CT reconstruction. Besides, the polygonal plates are arranged closely, that not only reduces the volume of CT device, but also avoids unnecessary X-ray dose radiation problem.

Based on the proposed specific CT architecture and scanning scheme, we develop corresponding algorithms to finish forward projection, projection data completion, and iterative reconstruction. Experimental results have shown that our system configuration can effectively reconstruct 3D object with high quality. Further, the novel combination of high-density X-ray sources devices and flat-detectors opens a door to design new stationary CT systems in practice.

REFERENCES

[1] G. Wang, H. Yu, and B. De Man, "An outlook on X-ray CT research and development," *Med. Phys.*, vol. 35, no. 3, pp. 1051–1064, Feb. 2008.
[2] Y. Li, Y. Sun, and J. T. W. Yeow, "Nanotube field electron emission: Principles, development, and applications," *Nanotechnology*, vol. 26, no. 24, Jun. 2015, Art. no. 242001.
[3] R. H. Baughman, "Carbon nanotubes—The route toward applications," *Science*, vol. 297, no. 5582, pp. 787–792, Aug. 2002.
[4] H. Sugie, M. Tanemura, V. Filip, K. Iwata, K. Takahashi, and F. Okuyama, "Carbon nanotubes as electron source in an X-ray tube," *Appl. Phys. Lett.*, vol. 78, no. 17, pp. 2578–2580, Apr. 2001.
[5] Y. Cheng, J. Zhang, Y. Z. Lee, B. Gao, S. Dike, W. Lin, J. P. Lu, and O. Zhou, "Dynamic radiography using a carbon-nanotube-based field-emission X-ray source," *Rev. Sci. Instrum.*, vol. 75, no. 10, pp. 3264–3267, Oct. 2004.
[6] X. Qian, A. Tucker, E. Gidcumb, J. Shan, G. Yang, X. Calderon-Colon, S. Sultana, J. Lu, O. Zhou, D. Spronk, F. Sprenger, Y. Zhang, D. Kennedy, T. Farbizio, and Z. Jing, "High resolution stationary digital breast tomosynthesis using distributed carbon nanotube X-ray source array," *Med. Phys.*, vol. 39, no. 4, pp. 2090–2099, Mar. 2012.
[7] G. Yang, R. Rajaram, G. Cao, S. Sultana, Z. Liu, D. Lalush, J. Lu, and O. Zhou, "Stationary digital breast tomosynthesis system with a multi-beam field emission X-ray source array," *Proc. SPIE*, vol. 6913, Mar. 2008, Art. no. 69131A.
[8] E. M. Quan and D. S. Lalush, "Three-dimensional imaging properties of rotation-free square and hexagonal micro-CT systems," *IEEE Trans. Med. Imag.*, vol. 29, no. 3, pp. 916–923, Mar. 2010.
[9] B. Gonzales, D. Spronk, Y. Cheng, A. W. Tucker, M. Beckman, O. Zhou, and J. Lu, "Rectangular fixed-gantry CT prototype: Combining CNT X-ray sources and accelerated compressed sensing-based reconstruction," *IEEE Access*, vol. 2, pp. 971–981, 2014.
[10] X. Pan, E. Y. Sidky, and M. Vannier, "Why do commercial CT scanners still employ traditional, filtered back-projection for image reconstruction?" *Inverse Problems*, vol. 25, no. 12, Dec. 2009, Art. no. 123009.
[11] D. Chen, X. Song, Z. Zhang, Z. Li, J. She, S. Deng, N. Xu, and J. Chen, "Transmission type flat-panel X-ray source using ZnO nanowire field emitters," *Appl. Phys. Lett.*, vol. 107, no. 24, Dec. 2015, Art. no. 243105.
[12] Z. Zhang, D. Chen, W. Chen, Y. Chen, X. Song, R. Zhan, S. Deng, N. Xu, and J. Chen, "Thermo-enhanced field emission from ZnO nanowires: Role of defects and application in a diode flat panel X-ray source," *Appl. Surf. Sci.*, vol. 399, pp. 337–345, Mar. 2017.
[13] L. Zhao, Y. Chen, Y. Liu, G. Zhang, J. She, S. Deng, N. Xu, and J. Chen, "Integration of ZnO nanowires in gated field emitter arrays for large-area vacuum microelectronics applications," *Current Appl. Phys.*, vol. 17, no. 1, pp. 85–91, Jan. 2017.
[14] B. Liu, J. Bennett, G. Wang, B. De Man, K. Zeng, Z. Yin, P. Fitzgerald, and H. Yu, "Completeness map evaluation demonstrated with candidate next-generation cardiac CT architectures," *Med. Phys.*, vol. 39, no. 5, pp. 2405–2416, Apr. 2012.
[15] T. Sun, R. Clackdoyle, J.-H. Kim, R. Fulton, and J. Nuyts, "Estimation of local data-insufficiency in motion-corrected helical CT," *IEEE Trans. Radiat. Plasma Med. Sci.*, vol. 1, no. 4, pp. 346–357, Jul. 2017.
[16] Y. Chen, Y. Xi, and J. Zhao, "A stationary computed tomography system with cylindrically distributed sources and detectors," *J. X-Ray Sci. Technol.*, vol. 22, no. 6, pp. 707–725, 2014.
[17] H. Yan, X. Mou, S. Tang, Q. Xu, and M. Zankl, "Projection correlation based view interpolation for cone beam CT: Primary fluence restoration in scatter measurement with a moving beam stop array," *Phys. Med. Biol.*, vol. 55, no. 21, pp. 6353–6375, Nov. 2010.
[18] E. Y. Sidky, C.-M. Kao, and X. Pan, "Accurate image reconstruction from few-views and limited-angle data in divergent-beam CT," *J. X-Ray Sci. Technol.*, vol. 14, no. 2, pp. 119–139, 2006.
[19] Y. Zhang and X. Mou, "Metal artifact reduction based on the combined prior image," 2014, *arXiv:1408.5198*. [Online]. Available: http://arxiv.org/abs/1408.5198
[20] T. Bai, H. Yan, X. Jia, S. Jiang, G. Wang, and X. Mou, "Z-index parameterization for volumetric CT image reconstruction via 3-D dictionary learning," *IEEE Trans. Med. Imag.*, vol. 36, no. 12, pp. 2466–2478, Dec. 2017.
[21] E. Y. Sidky and X. Pan, "Image reconstruction in circular cone-beam computed tomography by constrained, total-variation minimization," *Phys. Med. Biol.*, vol. 53, no. 17, pp. 4777–4807, Sep. 2008.
[22] D. Kim, S. Ramani, and J. A. Fessler, "Accelerating X-ray CT ordered subsets image reconstruction with Nesterov's first-order methods," in *Proc. Int. Meeting Fully 3D Image Reconstruction Radiol. Nucl. Med.*, 2013, pp. 5–22.
[23] Z. Wang, A. C. Bovik, H. R. Sheikh, and E. P. Simoncelli, "Image quality assessment: From error visibility to structural similarity," *IEEE Trans. Image Process.*, vol. 13, no. 4, pp. 600–612, Apr. 2004.
[24] W. P. Segars and B. M. W. Tsui, "MCAT to XCAT: The evolution of 4-D computerized phantoms for imaging research," *Proc. IEEE*, vol. 97, no. 12, p. 1954, Dec. 2009.
[25] S. Zhi, M. Kachelrieß, and X. Mou, "High-quality initial image-guided 4D CBCT reconstruction," *Med. Phys.*, vol. 47, no. 5, pp. 2099–2115, Jun. 2020.
[26] S. Zhi and X. Mou, "Motion artifacts reduction in 4DCBCT based on motion-compensated robust principal component analysis," *Proc. SPIE*, vol. 10573, Mar. 2018, Art. no. 1057348.

YITING DUAN was born in Shanxi, China, in 1994. She received the B.E. degree from Xi'an Jiaotong University, in 2017, where she is currently pursuing the master's degree with the Institute of Image Processing and Pattern Recognition. Her current research interests include developing CT algorithm and novel CT systems.

HAITAO CHENG was born in Sichuan, China, in 1992. He received the master's degree from Xi'an Jiaotong University, in 2018. His research interest includes flat-panel CT reconstruction algorithm.

KAI WANG was born in Shanxi, China, in 1993. He received the master's degree from Xi'an Jiaotong University, in 2018. His research interests include CT reconstruction and X-ray CT system design.

XUANQIN MOU (Senior Member, IEEE) has been with the School of Electronic and Information Engineering, Institute of Image Processing and Pattern Recognition (IPPR), Xi'an Jiaotong University, Xi'an, China, since 1987, where he has been an Associate Professor and a Professor, since 1997 and 2002, respectively. He is currently the Director of IPPR and the Director of the National Data Broadcasting Engineering and Technology Research Center. He has authored or coauthored over 200 peer-reviewed journal or conference papers. He was a recipient of the Yung Wing Award for Excellence in Education, the KC Wong Education Award, the Technology Academy Award for Invention by the Ministry of Education of China, and the Technology Academy Awards from the Government of Shaanxi Province, China. He served as a member of the 12th Expert Evaluation Committee for the National Natural Science Foundation of China, and the Executive Committee of the China Society of Image and Graphics, the Executive Committee of the Chinese Society for Stereology, and also serves as the Deputy Director of the CT Committee of the Chinese Society for Stereology.